RGNZ/MGPB

Equivalent Geological Strength Index (GSI) approach with application to rock mass slope stability

Rudarsko-geološko-naftni zbornik
(The Mining-Geology-Petroleum Engineering Bulletin)
UDC: 622.1, 622.2
DOI: 10.17794/rgn.2022.4.5

Original scientific paper

Raúl Pozo[1]
[1] *Ph.D. student, Department of Engineering, Pontifical Catholic University of Peru, Av. Universitaria 1801, San Miguel, Lima 15088, Perú, https://orcid.org/0000-0002-2726-2970*

Abstract
A considerable amount of slope stability analysis has been observed in jointed rock masses in which the GSI (Geological Strength Index) estimated at the outcropping level is considered input data to define the rock mass strength. However, this procedure is unsuitable when the rock outcrop scale and the slope scale are significantly different (e.g. open-pit slopes), resulting in an overestimated rock mass strength. For this reason, and in the absence of criteria to modify the GSI based on the scale effects, in this research, a new GSI version is proposed, called GSI_e or "equivalent GSI". To define an expression for obtaining the GSI_e in terms of the rock mass properties, comparative stability analyses were conducted in a series of hypothetical slopes using two approaches: the first considers the rock mass as a discontinuous medium of rock blocks separated by discontinuities; the second considers the rock mass as an equivalent continuous medium characterized by an equivalent GSI. For the adequate equivalent GSI value, evaluated in each analyzed slope, the safety factor and the failure surface are similar in both approaches. In conformity with the results, a GSI_e formulation in terms of the slope height, the spacing, the intact rock strength, the persistence, and the joint conditions has been proposed. Finally, the formulation was validated by applying it in five cases of mining slopes where the failure occurred.

Keywords:
scale effects; GSI; rock mass; rock mechanics; slope stability; geomechanical characterization

1. Introduction

In engineering practice, it is common to find global slope stability analysis in fractured rock masses, either using the limit equilibrium or the finite element method, in which the GSI index (**Hoek, 1994; Hoek et al., 1995**) evaluated at the outcropping-level (GSI_0) is considered as input data to define the rock mass resistance according to the Hoek-Brown failure criterion. However, this procedure is not considered adequate when the rock outcrop scale, where the field data collection has been conducted, and the slope dimensions are significantly different, resulting in a possible overestimation of the rock mass strength.

Particularly in the open-pit mining industry, where the most significant economic benefit is demanded, slopes with heights greater than 500 m can be found, where global failures are possible. Some of these failures were reported by **Hoek et al. (2000)**, **Read and Stacey (2009)**, **Hormazabal et al. (2013)**, and **Martin and Stacey (2013)**. In these cases, considering the GSI_0 value in the global slope stability analysis would be obtaining overestimated safety factors by not considering the reduction of the rock mass resistance when increasing the scale of analysis.

1.1. Problem statement

In **Figure 1**, the same rock mass is shown schematically in four scales due to increasing the slope height (h). In the first case (scale A), the rock mass is observed at the outcrop-level scale, with a defined structure and joint condition, and characterized with a GSI-1 index, classified as "blocky" according to **Hoek et al. (1995)**, **Marinos and Hoek (2000)**, and **Hoek et al. (2013)**.

Although the rock mass is the same, when increasing the slope height, the value of GSI-1 mapped at the rock outcrop level is not suitable to represent its behaviour in the other scales of analysis (scales B, C, and D in **Figure 1**). For example, in the scale D, the rock mass is very fractured, with a "disintegrated" classification, so it would not be correct to characterize it with the GSI-1 value; therefore, the GSI value must be reduced from GSI-1 to GSI-4; however, there are no practical criteria to quantify the reduction of this value, and it is often done empirically, or simply not done.

In **Figure 1**, the GSI reduction is mainly represented due to the rock mass structure, however, the joint condition is also affected by the scale effects when the real

Corresponding author: Raúl Pozo
e-mail address: raul.pozo@pucp.edu.pe

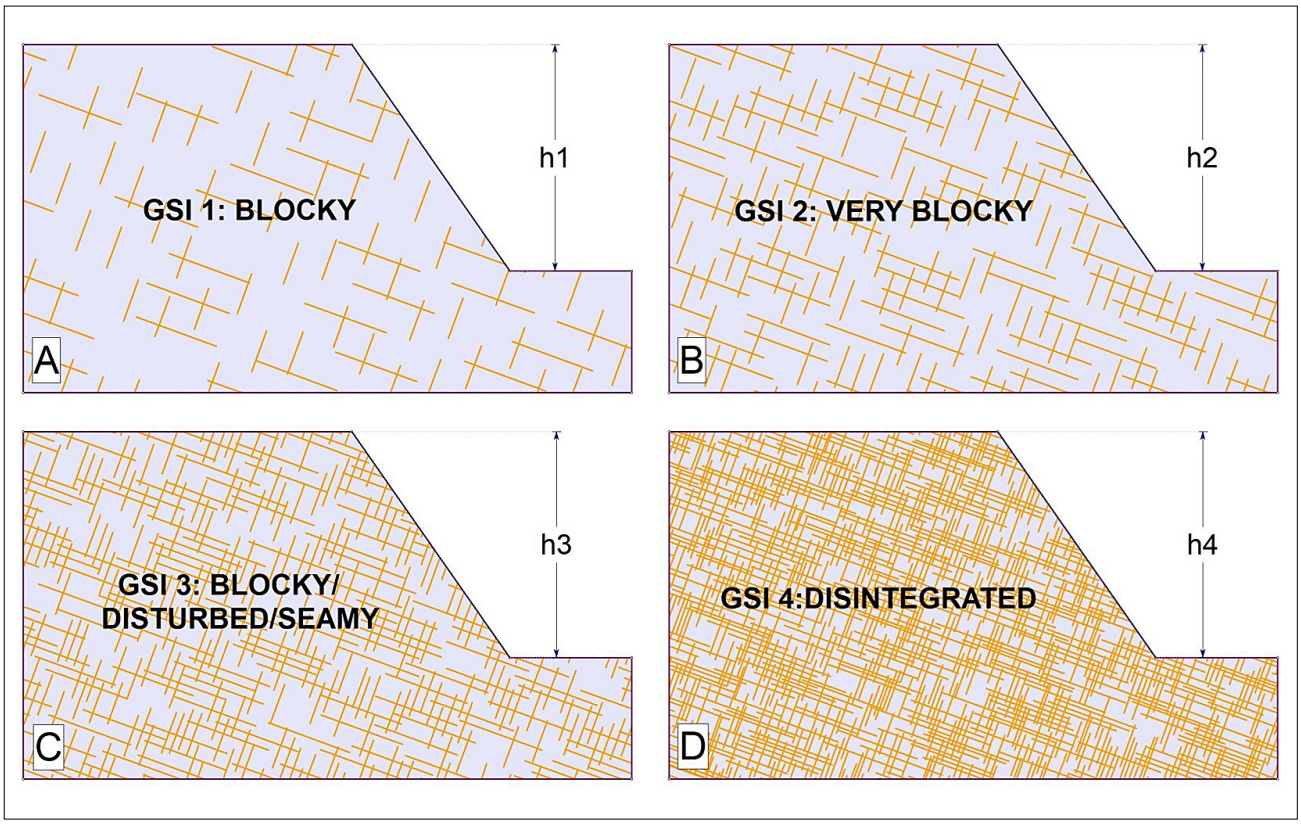

Figure 1: Rock mass slope with the same fractures network seen at different scales

joint length is considered. Following this approach, **Barton and Choubey (1977)** published an empirical failure criterion that considers the joint strength reduction depending on the scale of analysis (**Equation 1**).

$$\tau = \sigma_n \tan\left(JRC \log_{10}\left(\frac{JCS}{\sigma_n}\right) + \varphi_r \right) \quad (1)$$

Where:

φ_r – Residual friction angle,

JRC – Joint Roughness Coefficient,

JCS – Joint Wall Compression Strength.

In the context of the joint modelling, increased joint size caused marked reductions in JRC and JCS (**Barton et al., 1985**). To consider these size effects **Barton and Bandis (1982)** developed the formulations presented in **Equation 2** and **Equation 3**, the subscripts (0) and (n) are indicated for laboratory scale (L_0=10 cm) and in situ scale respectively.

$$JRC_n = JRC_0 \left(\frac{L_n}{L_0}\right)^{-0.02 JRC_0} \quad (2)$$

$$JCS_n = JCS_0 \left(\frac{L_n}{L_0}\right)^{-0.03 JRC_0} \quad (3)$$

Where:

JRC_0, JCS_0 – Refer to 10 cm laboratory scale samples,

JRC_n, JCS_n – Refer to in situ block sizes.

As a result, the GSI reduction when larger observation scales are considered is a function of both, the decrease in the block interlocking (rock mass structure) and the decrease in the joint condition. Consequently, the GSI reduction by scale effects would be reflected in the GSI chart published by **Hoek et al. (2013)** as a shift to the right and downwards (see **Figure 2**) when the slope height is increased, indicating the change in the rock mass structure and the joint condition from scale A to scale D, suggesting a reduction in the rock mass quality.

Therefore, the relationships presented in **Equation 4** and **Equation 5** are consistent.

$$h_1 < h_2 < h_3 < h_4 \quad (4)$$

$$GSI_1 > GSI_2 > GSI_3 > GSI_4 \quad (5)$$

Where:

h_i – Slope height at a given scale,

GSI_i – GSI associated with h_i.

According to the mentioned, the GSI should be modified to consider the scale effects, mainly conditioned by the relationship between the average joint spacing (e) and the slope height (h).

1.2. Why can we use the GSI value as a scale-dependent parameter?

The GSI system assumes that the rock mass is conformed by a sufficiently large number of joint sets and

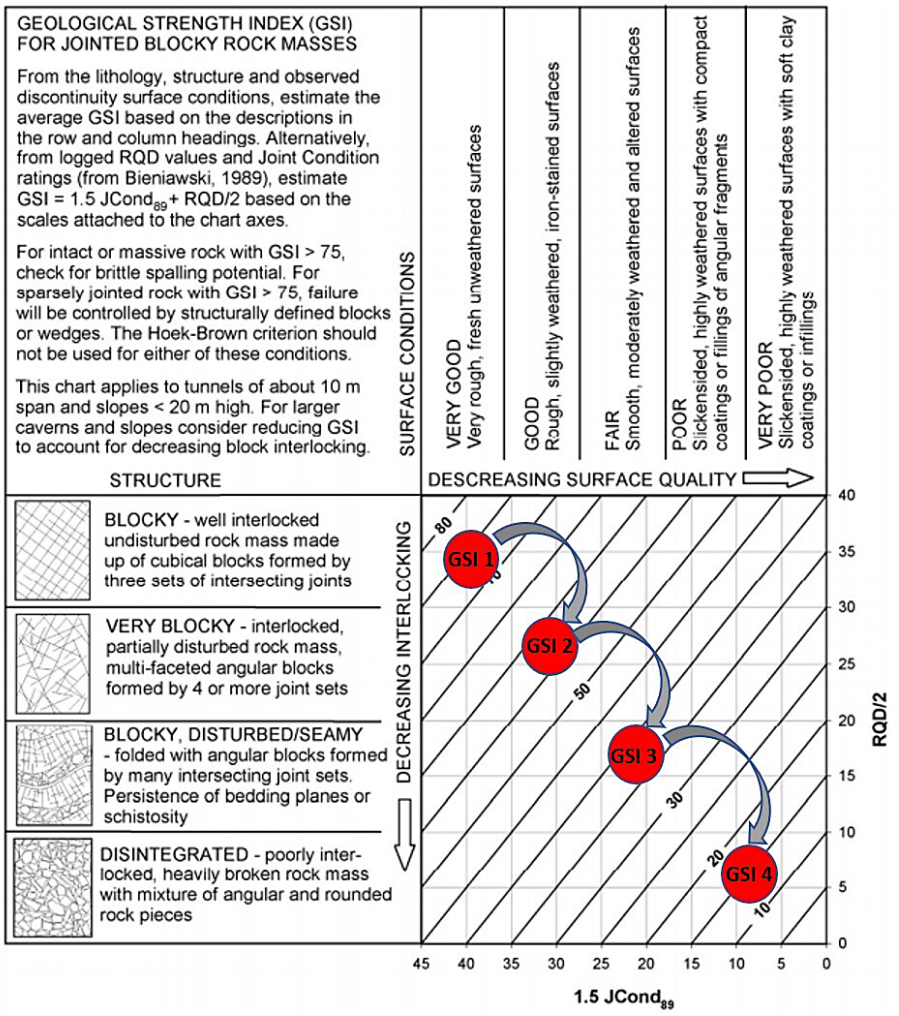

Figure 2: GSI reduction reflected in the GSI chart published by **Hoek et al. (2013)**

randomly oriented discontinuities; therefore, the rock mass can be treated as a homogeneous and isotropic mass of interlocking blocks, and the failure is a result of sliding along discontinuities or rotation of blocks (**Hoek and Brown, 2019**). To conclude if the rock mass could be considered continuous or discontinuous, not only the representative block size should be evaluated, additionally, the ratio of the size of the blocks to the size of the structure in which they exist is an important factor (**Hoek and Brown, 2019**). For example, **Hoek and Karzulovic (2000)** consider that the GSI index is not applicable when the individual block size is greater than a quarter of the excavation size, **Schlotferd and Carter (2018)** suggest that the GSI should not be used when the slope height or tunnel span is greater than three times the average fracture spacing.

The original GSI approach does not consider the scale effects since it is usually calculated quantitatively in terms of parameters that define the rock mass structure (RQD, block volume, SR) and the joint condition ($JCond_{89}$, SCR), which are defined at outcrop scale. However, these parameters can lose significance at larger scales, for example in a rock mass with an average joint spacing of 1m, the RQD value is 100%, corresponding to a rock mass with an excellent quality, whose failure would be governed by the disposition and resistance of the fractures; on the other hand, this rock mass evaluated on a 100 m slope height would present a different behaviour due to the relativity of the observation scale. While at the outcrop scale the joint spacing/height ratio is approximately 1/5-1/10, at a 100 m slope height the ratio is 1/100, which would determine the expected response of the rock mass. Similarly, it occurs with the discontinuities, where the roughness or waviness decreases when considering the large-scale persistence values. This consideration indicates that the GSI index would be considered as a scale dependency parameter on larger scales.

The recommendations regarding the reduction of the GSI due to scale effects have already been indicated in previous studies, the most outstanding corresponding to **Hoek et al. (2013)** who indicated: "This chart applies to tunnels of about 10 m span and slopes < 20 m high. For larger caverns and slopes consider reducing GSI to account for decreasing block interlocking". **Sonmez et al. (2021)** indicated that: "when the engineering dimension

(slope height, tunnel span) is increased, then a reduction in the GSI value should be expected". The use of the RQD or some variation of the volumetric joint count (J_v) or the block volume (V_b), limits the definition of rock structure to the dimension of the blocks. This takes no account of the ratio of block size to the size of the tunnel or slope which has a significant influence on the application of the GSI chart for characterizing the rock mass (**Sonmez et al., 2021**).

Mostyn and Douglas (2000) suggest that: "scale effects can be accounted for by interpreting the Geologic Strength Index (GSI) at the scale of interest. This requires the user to judge both the structure (as defined by blockiness and degree of interlocking) and the surface conditions (as defined by surface quality)". **Cundall et al. (2008)** suggested that the value of GSI should be estimated based on the relative scale of the problem, expressed as the number of blocks across the scale of interest.

The GSI reduction problem has also been studied considering the synthetic rock mass approach (**Mas Ivars et al., 2007**), for example, the study of the failure mechanism at various analysis scales (2m, 5m, 10m, and 20m) was carried out by **Elmo et al. (2011, 2016)** and **Schlotfeldt et al. (2017)**, who demonstrated how the synthetic rock mass could effectively capture the reduction in rock mass strength and define an equivalent GSI when the scale of analysis is increased. The results are shown in **Figure 3**, the Hoek-Brown curves (dashed lines) have been plotted assuming a variation of the GSI for a rock mass with UCS=50MPa and m_i=28, and conclude that the results clearly show how the synthetic rock mass model provides a reasonable estimate of rock mass strength. The GSI at the rock outcrop-level is 70, considering an evaluation window of approximately 4 m, which is reduced 10 points for an observation scale of 20 m.

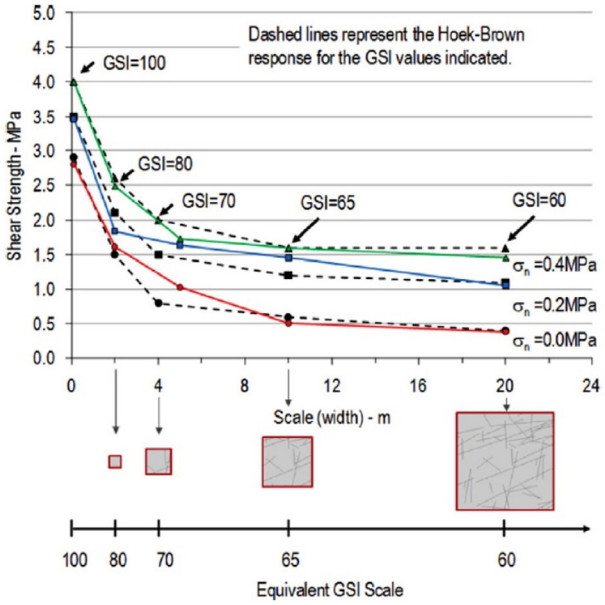

Figure 3: Variation of SRM strength and estimated correlation between strength and sample size (from **Schlotfeldt et al., 2017**)

Consequently, several researchers from different analysis approaches conclude that the GSI index should be reduced when the analysis scale is larger than the outcrop scale, and the importance of the spacing between fractures or the block volume is relevant, not as an independent parameter, but as a parameter that must be studied in relation to the size of the excavation.

1.3. Hypothesis

Due to the absence of a practical criterion to reduce the GSI based on the scale analysis, the present investigation proposes the definition of an equivalent GSI index (GSI_e), calculated with the following expression (**Equation 6**):

$$GSI_e = k * GSI_0 \quad (6)$$

Where:

GSI_0 – GSI value at the rock outcrop,
GSI_e – Equivalent GSI,
k – Scale reduction factor.

The parameter k depends on geometric and geomechanical features associated with the analyzed slope, mainly influenced by the *h/e* relationship, where *e* is the average spacing of the fractures, and *h* is the slope height. Therefore, the formulation proposed in this research has the form presented in **Equation 7**.

$$k = f\,(\textit{slope height, spacing, fracture network, UCS, structure, joint condition, etc.}) \quad (7)$$

The formulation proposed depends mainly on *e* and *h* for the reason that previous studies published by **Hammah et al. (2008, 2009)** suggest that the *h/e* relationship greatly influences the rock mass behaviour and the failure surface. When the *h/e* ratio is large, the slope tends to present a rotational behaviour at failure, similar to soils. When *e* and *h* are of the same order, structurally controlled failures are more likely, such as wedges or plane failures.

1.4. Literature review

GSI index is generally obtained visually, assessing two parameters: the rock mass structure and the joint condition. Subsequently, various attempts arose to quantify the GSI based on specific rock mass parameters, being the quantitative formulations of **Sonmez and Ulusay (2002)**, **Cai et al. (2004)**, **Russo (2009)**, and **Hoek et al. (2013)** as the most widespread; however, their application is limited to the rock outcrop scale.

Previous studies published by **Hoek et al. (1998)**, **Marinos and Hoek (2000)**, **Hoek et al. (2002)**, **Marinos et al. (2005)**, **Hoek et al. (2013)**, **Marinos and Carter (2018)**, and **Hoek and Brown (2019)**, provide essential recommendations on the application of the

GSI, refer to conditions of alteration, lithology, moisture, the opening of joints, filling and depth, but recommendations about scale effects are not presented.

In particular, **Hoek et al. (2013)** argued that GSI values calculated with the GSI charts or with the quantitative formulations are applicable for tunnels up to 10 m in span and slopes of heights less than 20 m, for large caverns and slopes, it is recommended to reduce the value of the GSI considering the loss of the interconnection of the rock blocks. However, **Hoek et al. (2013)** do not provide any practical criteria to reduce the GSI when some slopes or tunnels exceed the mentioned dimensions.

In addition, several authors have considered modifying the GSI from various approaches; for instance, **Day et al. (2016, 2019)** introduced the concept of the composite GSI (CGSI) that considers the intra-block structure of specific rock masses, **Russo et al. (2020)** proposed a chart to calculate GSI for rock masses in hypogenic environments, **Baczynski (2020)** define the directional GSI, including the influence of co-aligned fractures with unfavorable orientation in slopes with step-path failure, **Lin et al. (2014)** and **Shang et al. (2011)** provided charts to calculate the GSI in cores from drilling in granites and gneisses respectively, **Truzman (2009)** published an exclusive chart for application in metamorphic rocks.

Another group of publications included the GSI applications to evaluate specific rock mass properties, besides its resistance; for instance, **Mejía and Chacón (2019)** studied the relationship between the GSI and the support of tunnels, **Tsiambaos and Saraglou (2009)** studied the relation between GSI and the excavability of rock masses, **Kayabasi (2017)** related the GSI and the rock mass permeability, **Mesec et al. (2016)** characterized the ground vibrations level through the GSI index, **Špago and Jovanovsky (2019)** presented a criterion to evaluate the rock mass karsticity depending on the GSI and the porosity.

In conclusion, in the literature review, quantitative formulations that consider the GSI reduction due to the scale effects have not been found. Usually, a subjective reduction is applied, for example, reducing the GSI by 10 points, or reducing the GSI by one category referring to the rock mass structure. Although these criteria are simple and attempt to quantify the GSI reduction due to scale effects, their application is very subjective, since it does not consider the relationship between the joint spacing and the geometry of the analyzed structure.

Recently, **Sonmez et al. (2021)** proposed to decrease the Structure Ratio (SR) based on a reduction parameter s_f and a referential engineering dimension. SR represents the rock mass structure in the GSI formulation proposed by **Sonmez and Ulusay (1999, 2002)**, so applying a reduction factor is indirectly equivalent to reducing the GSI. Although this criterion does not consider modifying the joint condition, it constitutes an advance in the quantification of the GSI reduction. According to this approach, the present investigation proposes a quantitative formulation developed to directly reduce the GSI value.

2. Methods

Since small-scale laboratory experiments are not always representative of naturally jointed rock masses and large-scale in situ experiments are impractical, numerical modeling offers an alternative method to study jointed rock masses (**Xia et al., 2016**). According to **Day et al. (2022)**, in situations where explicitly modeling rock mass structures is not possible for reasons such as inadequate information from site investigation to determine appropriate input properties for joint elements or excessive computational demand where too many joint elements result in software crashes, modeling rock masses as equivalent continuum materials is a convenient solution.

For these reasons, numerical modeling was considered to define the analytical expression for the parameter k. Thereby, a series of hypothetical slopes were selected, represented by the slope geometry, the fracture networks, the properties of the rock matrix, and the discontinuities.

The numerical modeling has been conducted considering two approaches: in the first approach, the rock mass is modeled as a discontinuous medium of intact rock blocks separated by the discontinuities. In this case, the J-FEM Method or the finite element method with explicit representation of the discontinuities has been applied; this method represents the planes of the discontinuities as "joint type" finite elements, according to the formulation of **Goodman et al. (1968)**, which decomposes the contribution by inertia and by the damping of the joint elements. In **Figure 4(a)**, the original configuration of the model is presented, and in **Figure 4(b)**, the displaced configuration, where the nodes can move both normally and tangentially in regard to each other.

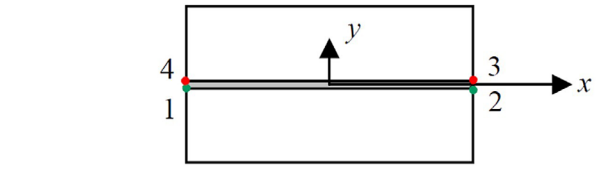

(a) Original configuration

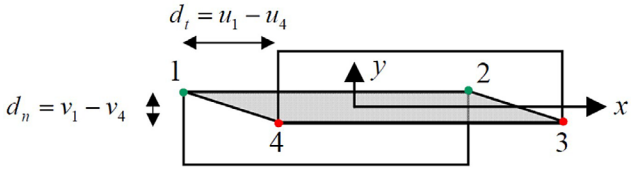

(b) Displaced configuration

Figure 4: The geometry of the finite joint element (**Goodman et al., 1968**): (a) in the original configuration; (b) in the displaced configuration (from **Riahi et al., 2010**)

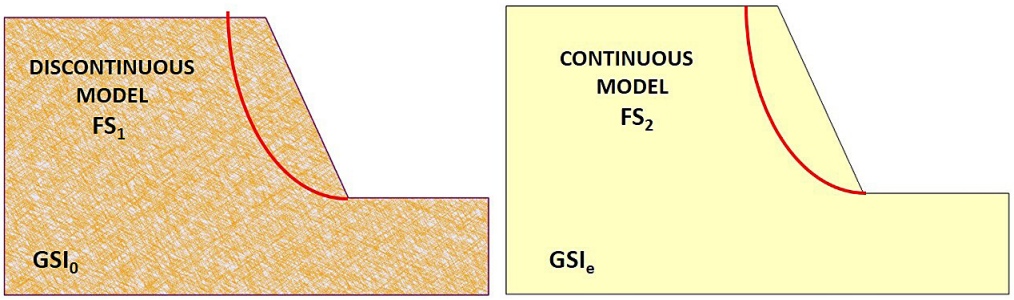

Figure 5: Comparison between the two analyzed approaches

The stiffness matrix [K] of the finite joint element is expressed in terms of the normal stiffness (k_n), the tangential stiffness (k_s), and the length of the discontinuity (l).

$$[K] = \frac{l}{6}\begin{pmatrix} 2k_s & 0 & 1k_s & 0 & -1k_s & 0 & -2k_s & 0 \\ 0 & 2k_n & 0 & 1k_n & 0 & -1k_n & 0 & -2k_n \\ 1k_s & 0 & 2k_s & 0 & -2k_s & 0 & -1k_s & 0 \\ 0 & 1k_n & 0 & 2k_n & 0 & -2k_n & 0 & -1k_n \\ -1k_s & 0 & -2k_s & 0 & 2k_s & 0 & 1k_s & 0 \\ 0 & -1k_n & 0 & -2k_n & 0 & 2k_n & 0 & 1k_n \\ -2k_s & 0 & -1k_s & 0 & 1k_s & 0 & 2k_s & 0 \\ 0 & -2k_n & 0 & -1k_n & 0 & 1k_n & 0 & 2k_n \end{pmatrix} \quad (8)$$

Hammah et al. (2008, 2009) demonstrated the versatility of the J-FEM method to represent the behaviour of jointed rock masses seen at different scales, validating this methodology by comparing it with the results from the application of the discrete element method. However, the limitations of the technique were later indicated by **Riahi et al. (2010)**, concluding that the J-FEM method adequately represents the behaviour of the rock mass in terms of the failure surface and the safety factor; despite the fact that the process does not generate the formation of new contacts between rock blocks; consequently, it is not recommended for evaluating large displacements. As a result, a safety factor (FS_1) and a potential failure surface are given.

The second approach considers the rock mass as an equivalent continuous medium evaluated with the limit equilibrium method according to Spencer's formulation and the generalized Hoek-Brown failure criterion (**Hoek et al., 2002**). Firstly, suppose that the stability analysis of the continuous model is conducted with the GSI_0 value, then it is most likely to reach higher safety factors than those obtained with the first approach ($FS>FS_1$). After that, the GSI_0 begins to be reduced through a sensitivity analysis until getting the value that provides both a similar safety factor and failure surface regarding the first approach results ($FS_1=FS_2$). Finally, the GSI that satisfies this condition is called GSI_e. The comparison of the results between the two analyzed approaches is presented schematically in **Figure 5**.

2.1. Analyzed cases

The hypothetical slopes, in which the comparison analyses have been conducted, were defined based on the slope geometry, the distribution of fracture networks, the properties of the intact rock, and the joint condition.

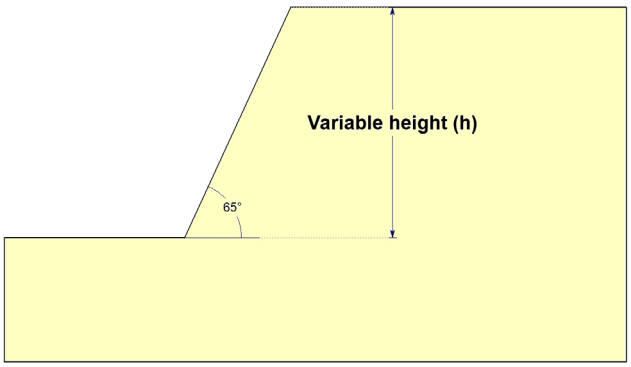

Figure 6: Trial slope (variable height)

2.1.1. Slope geometry

A general test slope with an inclination of 65° and a variable height of H = 250 m, 200 m, 150 m, 100 m, and 50 m has been considered to study the effect of the *e/h* ratio on the slope behaviour. Therefore, the modeling of a slope with a definite joint spacing has been analyzed with five different *e/h* ratios. The test slope is presented in **Figure 6**.

2.1.2. Fracture networks

Fifteen different fracture networks were defined as a result of combining four individual fracture systems: F1, F2, F3, and F4, associated them in groups of 1, 2, 3 and 4, resulting in the discrete fracture networks: F1, F2, F3, F4, F1F2, F1F3, F1F4, F2F3, F3F4, F2F4, F1F2F3, F1F4F4 F1F2F4, F2F3F4 and F1F2F3F4 (see **Figure 7**).

The F1 system is inclined 60° (counterclockwise), the F2 system is perpendicular to F1 (that is, at -30°), the F3 system is horizontal, and the F4 system is vertical.

2.1.3. Joint condition

Hoek et al. (2013) suggested five categories corresponding to very good, good, fair, poor, and very poor joint conditions. To assign the shear strength parameters to the mentioned groups, the proposal of **Pitts and Diederich (2011)** has been taken as a reference, which al-

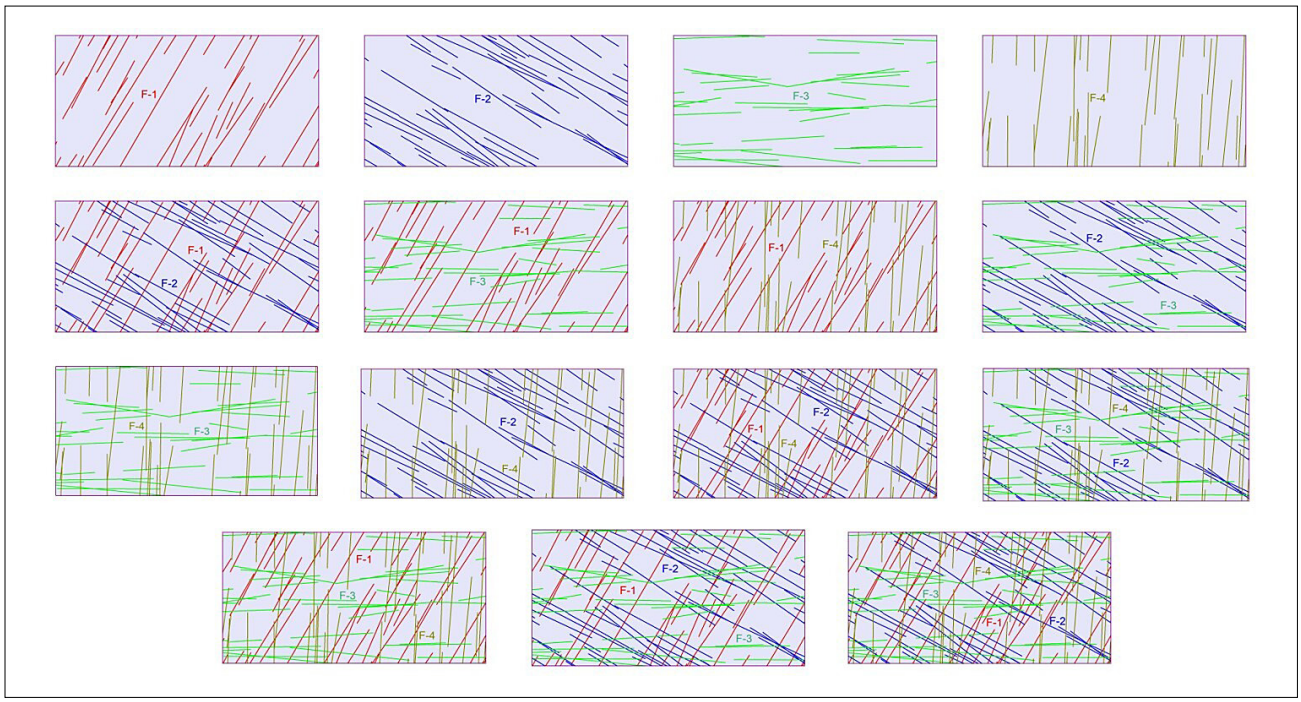

Figure 7: Analyzed fracture networks

Table 1: Resistance parameters depending on the joint condition

Joint Condition	JRC_0	JCS_0 (MPa)	Φ_r (°)
Very good	9 – 20 (14.5)	75 – 100 (87.5)	35 – 45 (40.0)
Good	8 – 14 (11.0)	55 – 75 (65.0)	30 – 35 (32.5)
Fair	2.3 – 11 (6.7)	40 – 55 (47.5)	24 – 30 (27.0)
Poor	0.9 – 7 (3.9)	20 – 40 (30.0)	18 – 24 (21.0)
Very poor	0.5 – 1.5 (1.0)	5 – 20 (12.5)	8 –18 (13.0)

Notes:
- The average values are presented in parentheses.
- Modified from **Pitts and Diederich (2011).**

lows characterizing the joint shear strength in terms of the parameters of **Barton and Choubey (1977)** criteria, such as JRC_0, JCS_0, and φ_r (see **Table 1**).

2.1.4. Intact rock properties

For the selection of the intact rock parameters, the recommendation of **Marinos and Carter (2018)** has been considered, which groups the rock masses into eight categories (see **Table 2**), based on the lithology, the uniaxial compressive strength UCS (10 MPa - 250 MPa), and the parameter m_i (4 -33).

At least on a preliminary level, this information can be used to characterize many rock masses found in nature. For more detail about specific rock masses, publications that present particular charts, such as **Marinos and Hoek (2000)**, **Hoek et al. (2005)**, or **Marinos (2017)**, could be reviewed.

2.1.5. Persistence

In accordance with the description of the joint persistence presented by the ISRM (**Brown, 1981**), five representative values have been considered (p = 1m, 3m, 10m, 20m, and 30m), corresponding to the limits of the mentioned classification. The summary of the analyzed cases with the combinations of the joint conditions defined by JRC_0 and JCS_0 (see **Table 1**) and the persistence values are presented in **Table 3**, the reduced JRC_n and JCS_n values considering the different persistences were calculated according to **Barton and Bandis (1982)**, presented in **Equation 2** and **Equation 3**.

2.1.6. Rock mass structure

The suggestion of **Hoek et al. (2013)** was considered to define the rock mass structure; this proposal considers four categories defined according to the RQD index (**Deere, 1963**): fractured in blocks (60 <RQD <80), intensely fractured in blocks (40 <RQD <60), fractured, sheared, or disturbed (20 <RQD <40) and disintegrated (RQD <20).

2.1.7. Resume

Finally, **Table 4** shows all the variables that will be included in the analyzed cases for the study of the scale effects on the slope stability. The analyzed cases have been obtained by combining the variables discussed, considering some representative cases resulting from these combinations.

Table 2: Typical values for UCS and m_i range of igneous, metamorphic and sedimentary rocks (from **Marinos and Carter, 2018**)

Typical UCS (MPa)	Metamorphic	Igneous			Sedimentary	mi
		Intrusive		Extrusive (Volcanic)		
		Felsic	Mafic			
125-250		Coarse (granite)				31-33
100-300	Granular texture (granulites, quartz, gneiss)	Medium (granodiorite, diorite)				28-30
85-350	Medium, amorphous (amphibolite, gneiss)		Coarse (gabbro, peridotite) (in ophiolites)	Mafic (basalt), intermediate (andesite), felsic (rhyolite)	Coarse (conglomerate – not clayey)	25-27
75-350	Fine, amorphous (hornfels, quarzite)		Medium (dolerite/ diabase) (in ophiolites)		Medium (quartz cemented, sandstone) sandstone members of flysch or molasse/greywacke)	17-20
50-200	Bended, gneissose (biotitic gneiss)		Fine (serpentinite) (in ophiolites)		Medium carbonates (limestone), sandstone	13-16
30-100	Foliated (schists, phyllite)				Fine (clastics)(siltstone/ siltstone members of flysch or molasse/tuff)	10-12
20-60	Strongly schistose (schist, phyllite)				Fine, calc-rock (chalk/marl and siltstone)	7-9
10-50	Mylonites				Ultrafine (claystone, mudstone/sheared siltstone, shale within flysch)	4-6

Table 3: JRC_n and JCS_n as a function of the persistence

Joint Condition	JRC_0	JCS_0 (MPa)	Φ_r (°)	Persistence (p)									
				1 m		3 m		10 m		20 m		30 m	
				JRC_n	JCS_n	JRC_n	JCS_n	JRC_n	JCS_n	JRC_n	JCS_n	JRC_n	JCS_n
Very good	14.5	87.5	40.0	7.44	32.14	5.41	19.93	3.81	11.80	3.12	8.73	2.77	7.32
Good	11.0	65.0	32.5	6.63	30.40	5.21	21.16	3.99	14.22	3.43	11.31	3.14	9.90
Fair	6.7	47.5	27.0	4.92	29.90	4.25	23.98	3.61	18.82	3.29	16.38	3.12	15.09
Poor	3.9	30.0	21.0	3.26	22.92	2.99	20.15	2.72	17.50	2.58	16.14	2.50	15.39
Very poor	1.0	12.5	13.0	0.95	11.67	0.93	11.29	0.91	10.89	0.90	10.66	0.89	10.53

3. Results

Hammah et al. (2008, 2009) indicated that the *h/e* ratio greatly influences the rock mass behaviour and the failure surface. Considering this, in **Figure 8**, the values of the scale factor *k* obtained for the analyzed slopes and the *h/e* ratio has been plotted, differentiating them by a color determined on the joint condition.

Apparently, **Figure 8** shows no pattern followed by the results that permit defining any trend; for the specific value of *h/e*, a wide range of associated *k* values indicates a notable variability.

It can also be observed that the values corresponding to the very good joint conditions (red triangles) tend to be located in the upper part of the graph. On the other hand, the values corresponding to the very poor joint condition (yellow circles) are located at the bottom, indicating a more significant reduction due to scale effects.

Therefore, to find a relationship or tendency in the results, these were grouped into five categories, corresponding to very good, good, fair, poor, and very poor joint conditions.

The division of the results is presented in **Figure 9**; it is observed that the results corresponding to the slopes that incorporate fracture networks with discontinuity F1 (red triangles), dipping unfavorably concerning the slope, are located in the lower part; and those that do not have F1 (green circles) are located in the top of the graph.

Moreover, considering this second association, it has been possible to observe an exponential trend curve for

Table 4: Summary of variables considered in slope stability analyses

Fracture networks[1]	Slope height H (m)	UCS[2] (MPa)	m_i[2]	Persistence p (m) [3]	Joint Condition[4]	Rock Mass Structure [5]
F1, F2, F3, F4	50	187.5	32.0	1	Very good	Blocky
F1F2, F1F3	100	200.0	29.0	3	Good	Very blocky
F1F4, F2F3	150	217.5	26.0	10	Fair	Blocky, disturbed/ seamy
F2F4, F3F4	200	212.5	18.5	20	Poor	Disintegrated
F1F2F3	250	125.0	14.5	30	Very poor	
F1F2F4		65.0	11.0			
F1F3F4		40.0	8.0			
F2F3F4		30.0	5.0			
F1F2F3F4						

Notes:
[1] Fracture networks were presented in **Figure 7**.
[2] The UCS and m_i values correspond to the average values of the eight groups suggested by **Marinos and Carter (2018)**, see **Table 2**.
[3] The persistence values were defined according to the description suggested by ISRM (**Brown, 1981**), for each persistence value, JRC_n and JCS_n were calculated according to the formulation of **Barton and Bandis (1982)**, see **Table 3.**
[4] The joint condition was defined based on the GSI chart published by **Hoek et al. (2013)**, and the strength properties associated with each category were defined by **Pitts and Diederich (2011)**, see **Table 1**.
[5] The rock mass structure was defined according to **Hoek et al. (2013)** and complemented with the description of **Cai et al. (2004)** who assigned spacing ranges to each rock mass category.

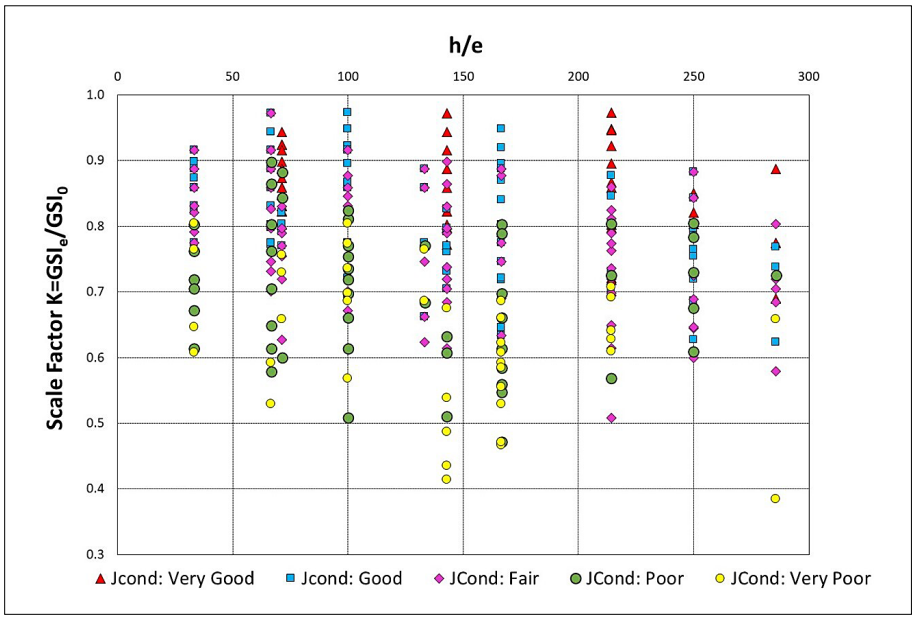

Figure 8: Results of all analyzed cases

both the data that include F1 or do not include the F1 system. These trend curves are shown dotted with red and green in **Figure 9**.

In general, the trend curves remarked suggest lower *k* values for a higher *h/e* ratio, indicating a more significant GSI reduction in conformity to a disintegrated rock mass behaviour; in addition, the presence of the F1 system induces an additional GSI reduction.

It is also observed that if the F1 system is not contemplated, the most unfavorable k values are in the order of 0.6, being notably lower in the cases in which the F1 system is taken into account. Consequently, there is an essential directional component to consider during the GSI reduction process, similar to that argued by **Baczynski (2020)**, who introduced the concept of directional GSI in the study of step-path failures in rock masses.

3.1. Proposed formulation

In conformity with the results obtained, an analytical formulation is proposed to calculate the scale factor *k*, defined as the relationship between GSI_e and GSI_0. From

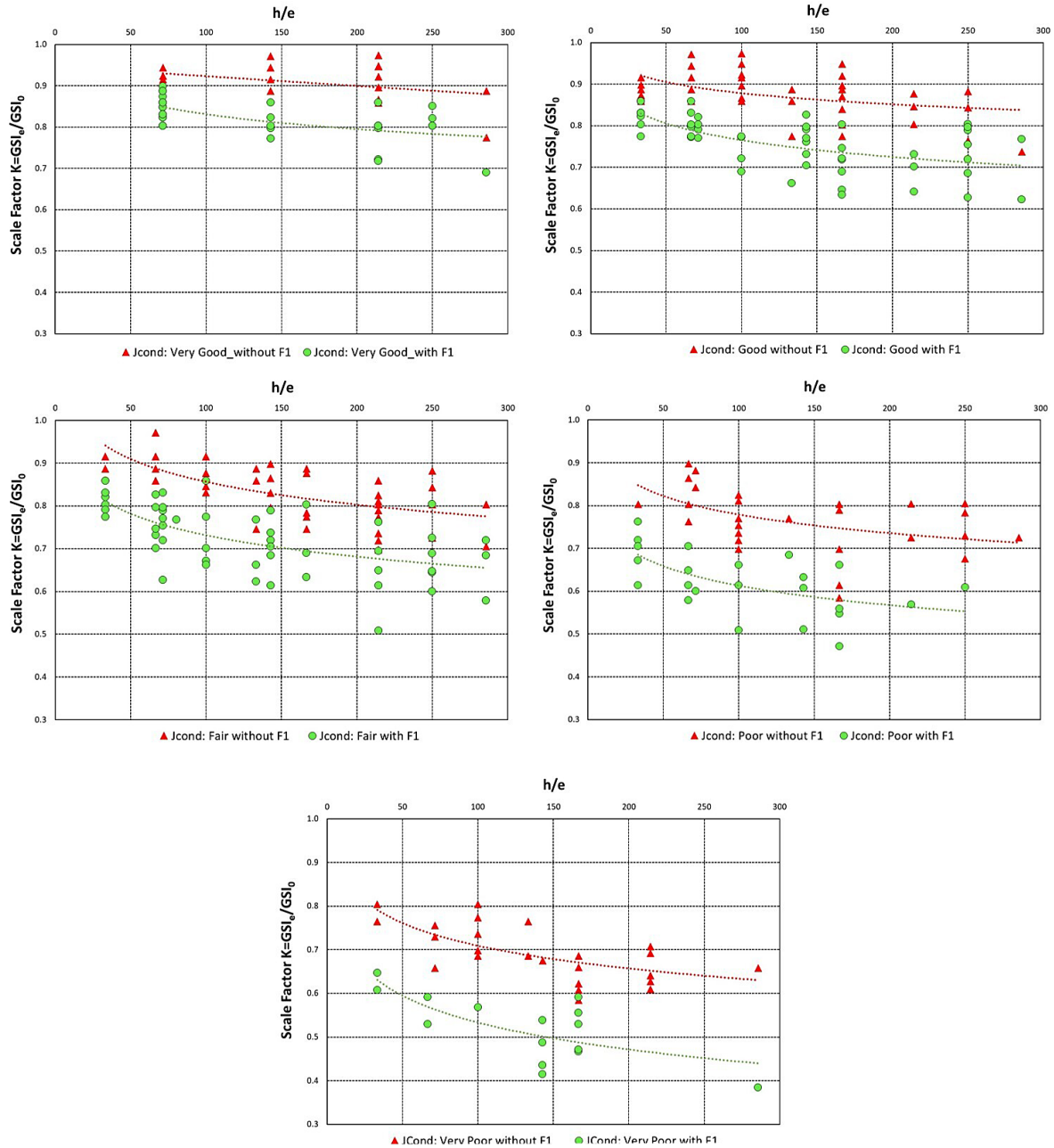

Figure 9: Results obtained as a function of the joint condition

the graphs presented in **Figure 9**, it is concluded that the proposed formulation must be expressed in terms of the *h/e* ratio, the joint condition, the directionality, and the GSI_0. As a result, the following formulation is proposed:

$$k = w_0 w_1 w_2 \left(\frac{h}{e}\right)^{-w_3 w_4} - w_5 \qquad (9)$$

Where:

k – Scale reduction factor,
w_0 – Parameter that depends on the slope height,
w_1 – Parameter that depends on the strength and stiffness of the intact rock,
w_2 – Parameter that depends on the persistence of the discontinuities,
w_3 – Parameter that depends on the directionality,
w_4 – Parameter that depends on the joint condition,
w_5 – Parameter that depends on the GSI_0,
h – Slope height [m],
e – Average spacing of discontinuities [m].

The suggested values of the parameters w_0, w_1, w_2, w_3, w_4, and w_5 are presented in **Table 5.**

3.2. Validation

To validate the proposed formulation, four mining slopes in Turkey were analyzed, in which the rock mass failure occurred. The characterization and analysis of these slopes are presented in **Sonmez et al. (1998), Son-**

Table 5: Parameters to calculate the scale factor *k*

Slope height (h)	w_0	**Strength and stiffness of the intact rock**	w_1
h>20m	1.00	m_i>19	1.15
h ≤20m	2.00	m_i ≤19	1.00
Persistence (m)	w_2	Unfavorably fractures (F1)	w_3
30	1.00	Yes	1.00
10	1.05	No	0.50
1	1.11		
Joint condition	w_4 [(1)]	Slope height (h)	w_5
Very good	0.03–0.07 (0.05)	h> 20m	0.43-0.006*GSI_0≥0
Good	0.04–0.10 (0.07)	h ≤20m	0.00
Fair	0.05–0.13 (0.09)		
Poor	0.08–0.15 (0.12)		
Very poor	0.10–0.18 (0.14)		

Notes:
[(1)] The average values are presented in parentheses.

mez and Ulusay (1999, 2002), and **Dinc et al. (2011)**. A fifth case corresponds to a natural slope located in Ancash-Peru, in which the rock mass has not broken.

Firstly, the general description of the slopes is presented; next, the *k* values are calculated as the ratio between GSI_e and GSI_0, this is called k_{real}; subsequently, the *k* values are calculated by the proposed formulation, designated as k_{calc}. Finally, the discrepancy between both results is compared in each analyzed slope.

In cases 1 to 4, slope failure has occurred, so it is possible to evaluate through a sensitivity analysis the GSI value that caused the failure (GSI_e), which is not necessarily equal to the reported during the field data collection (GSI_0). Case 5 is different; the slope has not failed, so the GSI_e value cannot be estimated at the failure condition; for this reason, firstly, the analysis of the rock mass has been conducted as a discontinuous medium (J-FEM approach), calculating a safety factor and defining a failure surface; subsequently, the sensitivity analysis focuses on finding the GSI value that provides a safety factor similar to that obtained with the discontinuous model, this is the value of GSI_e.

3.2.1. Case 1: Eskihisar Mine

This case history involves the instability of a slope of the Eskihisar Mine, a coal mine located in southwestern Turkey. According to **Sonmez and Ulusay (1999, 2002)**, the landslide occurred due to external loads from the construction of a temporary pile of rubble in the upper part of the slope. The GSI_0 value associated with the rock mass is 43.

In this case, the limit equilibrium reaches a safety factor very close to unity (see **Figure 10**) which indicates that the value of GSI_0=43 is adequate to represent the rock mass failure.

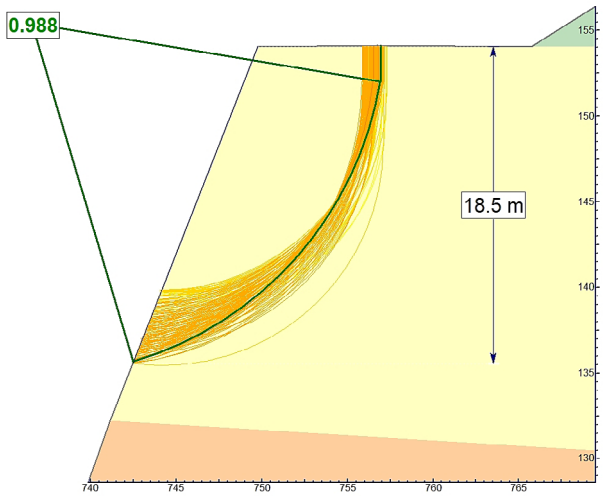

Figure 10: Slope stability of the Eskihisar Mine (GSI_o=GSI_e=43)

In this modeling, the slope failure occurred using directly the GSI reported in-situ (GSI_0=43). Hence, reducing the GSI for scale effects is unnecessary since this GSI value adequately represents the slope behaviour. Therefore, the value of k_{real} is calculated as:

$$k_{real} = \frac{GSI_e}{GSI_0} = \frac{43}{43} = 1.00 \qquad (10)$$

3.2.2. Case 2: Baskoyak Mine

Sonmez and Ulusay (1999, 2002) published the results of a comprehensive slope stability analysis conducted at the Baskoyak open-pit mine in western Anatolia, Turkey. Due to the intensely fractured nature of the rock mass, it was considered to be homogeneous and

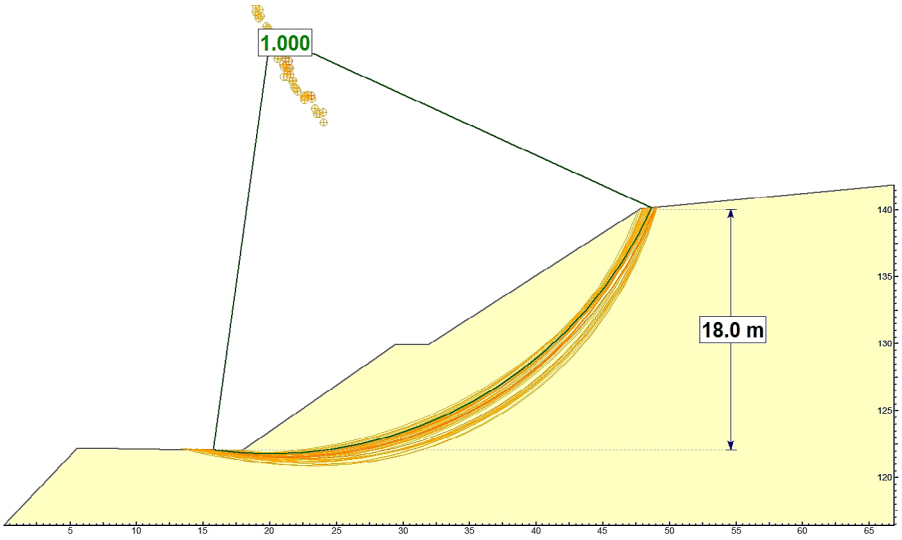

Figure 11: Slope stability of the Baskoyak Mine (GSI_e=15)

isotropic, with a fracture spacing of 0.04 m in all directions. The GSI_0 associated is 16.

For a GSI_0=16, the safety factor reached was 1.04, which indicates that the slope is very close to the failure. Subsequently, a sensitivity analysis established that a unitary safety factor was obtained for a value of GSI_e=15 (see **Figure 11**).

In this case, the GSI reduction attributable to scale effects is not significant since there is only one point of difference between GSI_0 and GSI_e. Therefore, it may be considered that the GSI value mapped at the rock outcrop level is adequate to represent the rock mass behaviour in the evaluated scale.

The value of k_{real} is calculated as:

$$k_{real} = \frac{GSI_e}{GSI_0} = \frac{15}{16} = 0.94 \qquad (11)$$

3.2.3. Case 3: Kiskadere Mine

Sonmez and Ulusay (1999) reported a study of the instability of the Kisrakdere open pit slope located in the lignite basin of Soma (Turkey). The rock mass of compact marl was reported as intensely fractured, with three systems of discontinuities, with slight or moderate spacing, presence of stratification planes in the opposite direction to the slope in the marly sequence (**Sonmez and Ulusay, 1999**). The GSI value mapped on the surface was 37 (GSI_0=37).

The stability analysis was conducted with the value of GSI_0=37, obtaining a safety factor of 1.38 (see **Figure 12**), considerably far from the unit safety factor that would produce the slope failure. Consequently, a sensitivity analysis was conducted, looking for the GSI value that provides a unit safety factor; the value obtained was 27 points (see **Figure 13**).

Unlike the two previous cases, the variation of the GSI values is 10 points, indicating associated scale effects. The k_{real} value indicates a reduction of GSI by 27%, which is calculated as:

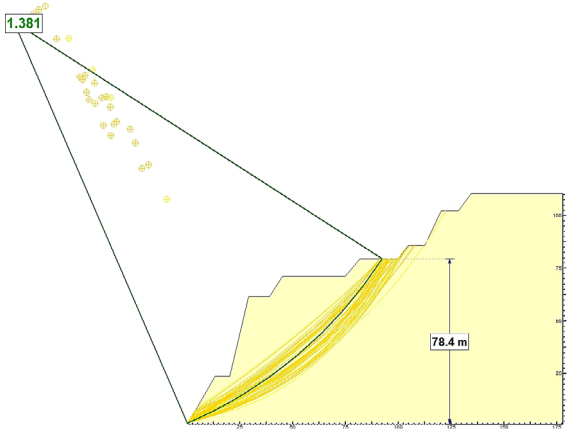

Figure 12: Slope stability of the Kiskadere Mine (GSI_o=37, FS=1.38)

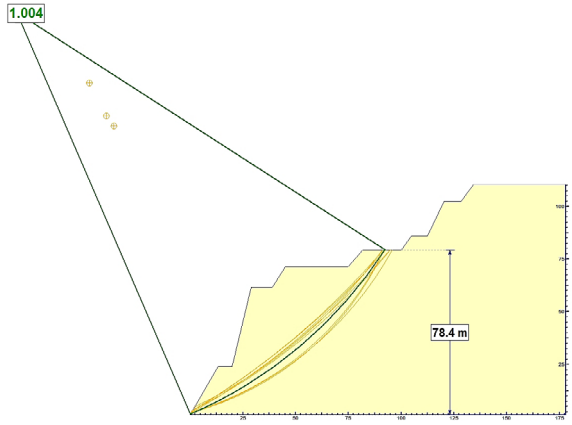

Figure 13: Slope stability of the Kiskadere Mine (GSI_o=27, FS=1.00)

$$k_{real} = \frac{GSI_e}{GSI_0} = \frac{27}{37} = 0.73 \qquad (12)$$

3.2.4. Case 4: Cayeli-Catampasa slope

Dinc et al. (2011) studied an andesite rock slope's instability located between Cayeli and Katampasa in Tur-

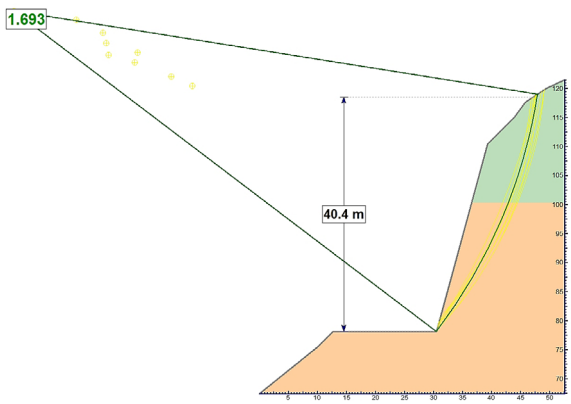

Figure 14: Slope stability of the Cayeli-Catampasa slope (GSI_o=58, FS=1.69)

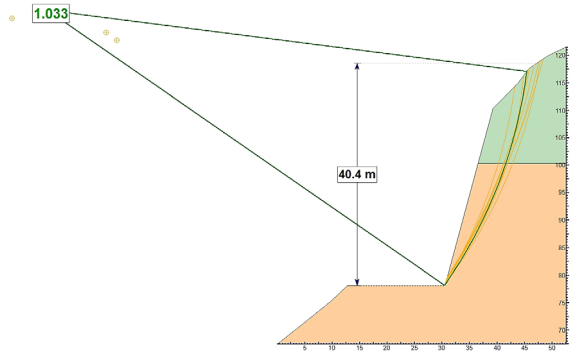

Figure 15: Slope stability of the Cayeli-Catampasa slope (GSI_o=25, FS=1.03)

key. The slope was excavated as a quarry to produce rocks for road construction and comprises two well-differentiated horizons. The upper part of the slope is moderately altered, while the lower part presents a slight to moderate alteration (**Dinc et al., 2011**).

According to **Dinc et al. (2011)**, the GSI_0 value associated with the rock mass is 37 in the upper part and 40 in the lower part of the slope. In this case, the stability analysis was performed using the limit equilibrium method, obtaining a safety factor of 1.69 (see **Figure 14**), which is considerably far from the safety factor equal to 1.0 that would produce the failure. Subsequently, a sensitivity analysis of the GSI was performed, looking for the value that provides a unit safety factor. The sought value is GSI_e=25 (see **Figure 15**).

In this case, the k_{real} value indicates a 34% reduction in the GSI value, which is calculated as:

$$k_{real} = \frac{GSI_e}{GSI_0} = \frac{25}{38} = 0.66 \qquad (13)$$

3.2.5. Case 5: Limestone rock slopes

The proposed methodology has been applied to evaluate the stability of three representative sections of a limestone slope with three fracture systems and GSI_0=58. Unlike the previous four cases, the failure has not occurred on these slopes, so it is not appropriate to calculate the value of k_{real} for the condition of FS=1.0. Therefore, the safety factors and the failure surface were previously defined with the J-FEM method since the analysis with explicit fracture networks is a better approximation than an equivalent continuous method.

Figures 16, 17, and 18 present the results considering the fracture networks and the continuous equivalent analysis, for which the safety factors and the failure surfaces are similar. In all three cases, it is observed that the safety factors vary between 2.19 and 2.80, which indicates an acceptable degree of stability and an approximately circular failure surface shape.

In the three representative sections, it is necessary to reduce the GSI_0 values to obtain similar results with the

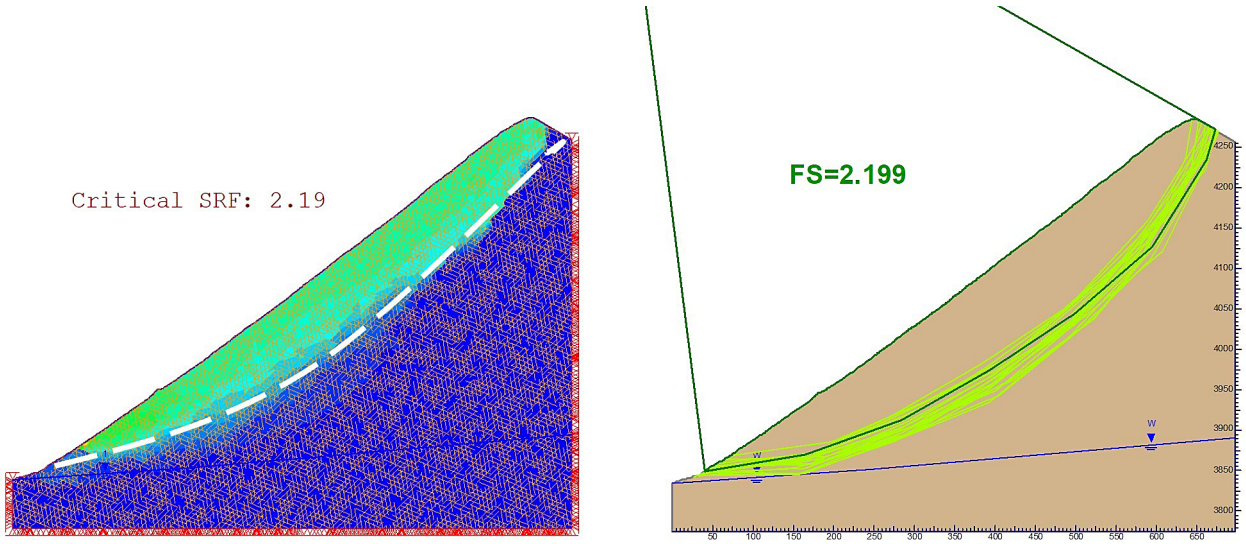

Figure 16: Analysis of section 1. Comparison of results between discontinuous (GSI_o=58) and equivalent continuous (GSI_e=35) models

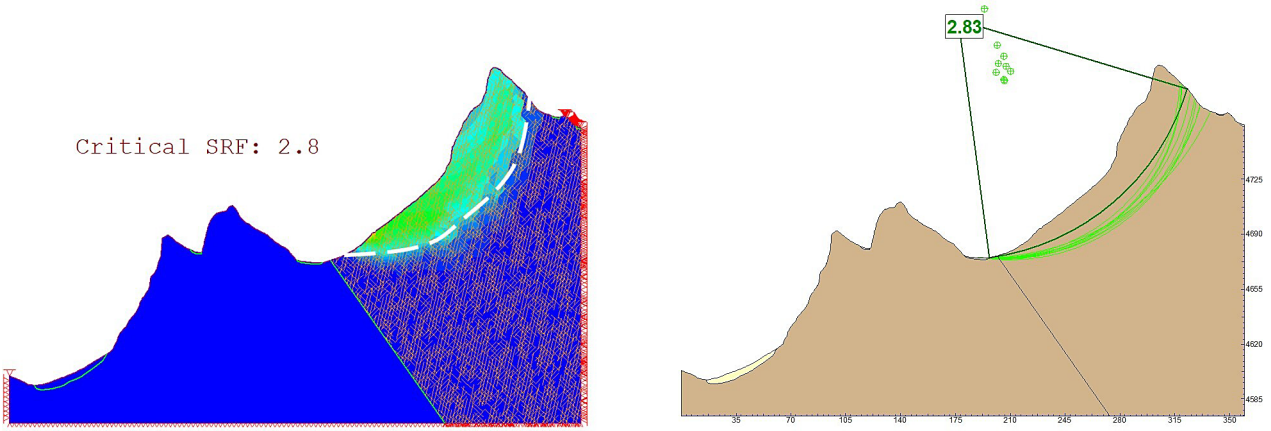

Figure 17: Analysis of section 2. Comparison of results between discontinuous (GSI_o=58) and equivalent continuous (GSI_e=35) models

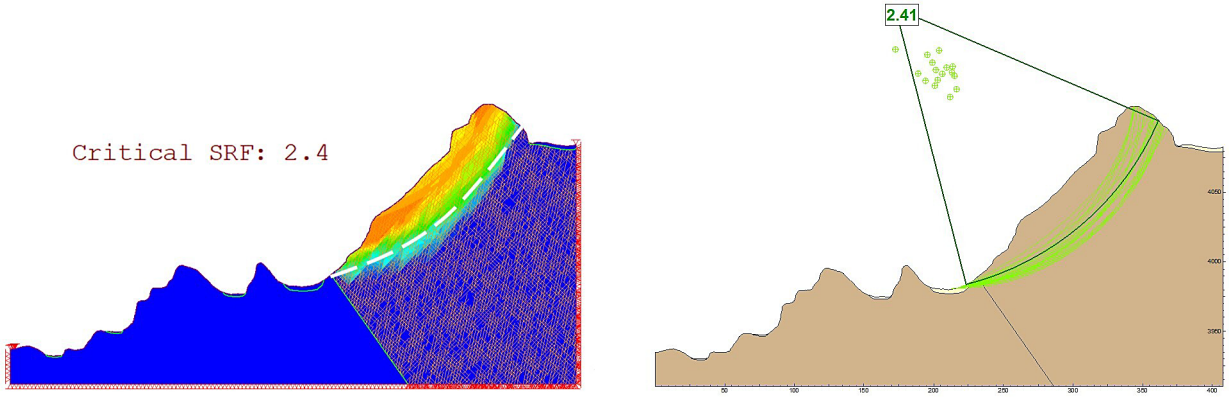

Figure 18: Analysis of section 3. Comparison of results between discontinuous (GSI_o=58) and equivalent continuous (GSI_e=40) models

J-FEM approach and the continuous equivalent model, which is an indicator of the scale effects associated. The GSI reduction due to scale effects is between 31% and 40%, which is associated with the considerable slope heights. The *k* values are the following:

$$k_{real-section1,section2} = \frac{GSI_e}{GSI_0} = \frac{35}{58} = 0.60 \quad (14)$$

$$k_{real-section3} = \frac{GSI_e}{GSI_0} = \frac{40}{58} = 0.69 \quad (15)$$

4. Discussion

The analyzed cases presented slopes influenced to different degrees by scale effects, quantified by the scale reduction factor *k*. In cases 1 and 2, the GSI reduction due to scale effects is negligible because the slopes have a height in the order of 18 m, which can be considered as a rock outcrop-level, that results are compatible with **Hoek et al. (2013)**, who argued that the reduction of the GSI value should be regarded for slopes above 20 m. Cases 3 and 4, corresponding to slopes with heights in the order of 40 - 70 m, present a GSI reduction of 27% to 34%, this reduction could be more significant if the fracture systems were dipping unfavorably concerning the slope face. Case 5 presents a GSI reduction of 31% to 40%; this reduction is justified due to the considerable slope height, their fracturing degree, and the presence of fracture systems dipping unfavorably concerning the slope face.

The k_{real} calculation has been presented for each case, obtained directly from the relation between GSI_0 and GSI_e; the process was uncomplicated in cases 1, 2, 3, and 4, where information about slope failure is available. In contrast, in case 5, the process was tedious and not practical since it involves performing numerical modeling with fracture networks. Due to these drawbacks, a reliable formula to obtain *k* directly was developed and validated (k_{calc}).

The results from all cases are summarized in **Table 6**, where the k_{real} and k_{calc} are indicated. It is observed that there is a similarity between both values of *k*, which shows an acceptable approximation of the proposed formulation.

The most significant difference between the results is observed in case 3, with a discrepancy of 0.13. However,

Table 6: Results of all analyzed cases

Parameter	Case 1	Case 2	Case 3	Case 4	Case 5		
	Eskihisar Mine	Baskoyak Mine	Kiskadere Mine	Cayeli - Catampasa	Section 1	Section 2	Section 3
w_0	2.00	2.00	1.00	1.00	1.00	1.00	1.00
w_1	1.00	1.00	1.00	1.15	1.00	1.00	1.00
w_2	1.05	1.00	1.00	1.05	1.00	1.00	1.00
w_3	1.00	1.00	0.50	1.00	1.00	1.00	1.00
w_4	0.09	0.12	0.09	0.09	0.05	0.05	0.05
w_5	0.00	0.00	0.21	0.21	0.082	0.082	0.082
H (m)	18.5	18.0	78.0	40.0	450.0	125.0	122.0
e (m)	0.85	0.04	0.60	0.35	0.60	0.60	0.60
GSI_0	43	16	37	38	58	58	58
GSI_e	43	15	27	25	35	35	40
ΔGSI	0	1	10	13	23	23	18
k_{calc}	1.00	0.96	0.60	0.58	0.63	0.68	0.68
k_{real}	1.00	0.94	0.73	0.66	0.60	0.60	0.69
| Error |	0.00	0.02	0.13	0.08	0.03	0.08	0.01

this difference does not imply a considerable variation. On the other hand, it is recommended that the value of *k* be defined as a range instead of a single value due to the uncertainty and variability that some input parameters could have, such as the rock mass structure and joint condition.

5. Conclusion

The formulation proposed in this work contributes to the quantification of the rock mass quality reduction as a consequence of the associated scale effects, for which the equivalent GSI index (GSI_e) has been defined, whose application is exclusive to problems involving slope stability in fractured rock masses.

The GSI_e index can be directly included in slope stability analyses performed by limit equilibrium or finite element methods. This index depends mainly on the *h/e* ratio, the presence of planes that dip unfavorably concerning the slope face, the fracture network, and the joint condition.

It is advisable to consider a range of values of the GSI_e instead of a single value due to the uncertainty and variability of the rock mass parameters, such as the condition of the discontinuities or their spacing.

For future studies, it would be convenient to analyze and modify the formulation proposed for its application in problems involving underground excavations or foundations in rock masses.

It is also advisable to consider the approach proposed in this research for the study of the UCS reduction depending on the scale analysis, keeping the GSI as a "constant" value. This would allow the introduction of a new scale factor relating values of the compressive rock mass strength and the intact rock strength.

6. References

Baczynski, N. (2020): Hoek–Brown rock mass: Adjusting geological strength index for Directional Strength. In: PM Dight, Slope Stability 2020 (ed.): Proceedings of the 2020 International Symposium on Slope Stability in Open Pit Mining and Civil Engineering - Australian Centre for Geomechanics, 901-912, 12 p. doi:10.36487/acg_repo/2025_59

Barton, N. and Choubey, V. (1977): The shear strength of rock joints in theory and practice. Rock Mechanics Felsmechanik Mecanique Des Roches, 10, 1-54. doi:10.1007/bf01261801

Cai, M., Kaiser, P., Uno, H., Tasaka, Y. and Minami, M. (2004): Estimation of rock mass deformation modulus and strength of jointed hard rock masses using the GSI system. International Journal of Rock Mechanics and Mining Sciences, 41, 1, 3-19. doi:10.1016/s1365-1609(03)00025-x

Cundall, P., Pierce, M. and Mas Ivars, D. (2008): Quantifying the size effect of rock mass strength. In: Proceedings of the First Southern Hemisphere International Rock Mechanics Symposium.

Day, J.J. (2022): How to incorporate variability of rockmass structures into equivalent continuum numerical models using the Composite Geological Strength Index. In: Hammah, R.E., Yacoub, T.E., McQuillan, A. and Curran, J. (eds.): Proceedings of the Rocscience International Conference – The Evolution of Geotech, 25 Years of Innovation. – CRC Press, Balkema, 110-116, 7 p. doi: https://dx.doi.org/10.1201/9781003188339

Day, J.J, Diederichs, M.S. and Hutchinson, D.J. (2016): Validation of Composite Geological Strength Index for healed rockmass structure in deep mine access and production

tunnels. In: Tunneling Association of Canada, 2016 Annual Conference, Capitalizing on Underground Infrastructure, 8 p.

Day, J.J., Diederichs, M.S. and Hutchinson, D.J. (2019): Composite Geological Strength Index approach with application to hydrothermal vein networks and other Intrablock structures in complex Rockmasses. Geotechnical and Geological Engineering, 37, 6, 5285-5314. doi:10.1007/s10706-019-00980-4

Deere, D.U. (1963): Technical description of rock cores for engineering purposes. Rock Mechanics and Engineering Geology, 1, 1, 16-22.

Dinc, O., Sonmez, H., Tunusluoglu, C. and Kasapoglu, K. (2011): A new general empirical approach for the prediction of rock mass strengths of soft to hard rock masses. International Journal of Rock Mechanics and Mining Sciences, 48, 4, 650-665. doi:10.1016/j.ijrmms.2011.03.001

Elmo, D., Schlotfeldt, P., Beddoes, R. and Roberts, D. (2011): Numerical simulations of scale effects under varying loading conditions for naturally fractured rock masses and implications for rock mass strength characterization and the design of overhanging rock slopes. In: Proceedings of the 45th US Rock Mechanics/Geomechanics Symposium. American Rock Mechanics Association.

Elmo, D., Moffitt, K. and Carvalho, J. (2016): Synthetic Rock Mass modelling: Experience gained and lessons learned. In: Proceedings of the 50th US Rock Mechanics/Geomechanics Symposium. American Rock Mechanics Association.

Goodman, R.E., Taylor, R.L. and Brekke, T.L. (1968): A model for the mechanics of jointed rock. Journal of the Soil Mechanics and Foundations Division, 94, 3, 637-659. doi:10.1061/jsfeaq.0001133

Hammah, R.E., Yacoub, T.E., Corkum, B. and Curran, J.H. (2008): The Practical Modelling of Discontinuous Rock Masses with Finite Element Analysis. In: Proceedings of the 42nd U.S. Rock Mechanics Symposium - 2nd U.S. - Canada Rock Mechanics Symposium, San Francisco, 8 p.

Hammah, R.E., Curran J.H. and Yacoub, T. (2009): Variation of Failure Mechanics of Slopes in Jointed Rock Masses with Changing Scale. In: Proceedings of the 3rd CANUS Rock Mechanics Symposium, Toronto, 8 p.

Hoek, E. (1994): Strength of rock and rock masses. International Society for Rock Mechanics News Journal, 2, 2, 4-16.

Hoek, E. and Brown, E. (2019): The Hoek–Brown failure criterion and GSI – 2018 edition. Journal of Rock Mechanics and Geotechnical Engineering, 11, 3, 445-463. doi:10.1016/j.jrmge.2018.08.001

Hoek, E., Carranza-Torres, C.T. and Corcum, B. (2002): Hoek-Brown failure criterion - 2002 edition. In: Reginald Hammah (ed.): Proceedings of the 5th North American Rock Mechanics Symposium and the 17th Tunneling Association of Canada Conference – NARMS-TAC 2002, 267-273, 8 p.

Hoek, E., Carter, T.G. and Diederichs, M.S. (2013): Quantification of the Geological Strength Index chart. In: Pyrac-Nolte, L.J. (ed.): Proceedings of the 47th US Rock Mechanics/Geomechanics Symposium ARMA – Curran Associates Inc., 9 p.

Hoek, E., Kaiser, P.K. and Bawden, W.F. (1995): Support of Underground Excavations in Hard Rock. Balkema, A.A., Rotterdam, 228 p.

Hoek, E. and Karzulovic, A. (2000): Rock mass properties for surface mines. In: Hustralid, W.A., McCarter, M.K. and Van Zyl D.J.A. (eds.): Slope Stability in Surface Mining, Littleton, Colorado: Society for Mining, Metallurgical and Exploration (SME), 59-70, 11 p.

Hoek, E., Marinos, P. and Benissi, M. (1998): Applicability of the Geological Strength Index (GSI) classification for very weak and sheared rock masses. The case of the Athens Schist Formation. Bulletin of Engineering Geology and the Environment, 57, 2, 151-160. doi:10.1007/s100640050031

Hoek, E., Marinos, P. and Marinos, V. (2005): Characterisation and engineering properties of tectonically undisturbed but lithologically varied sedimentary rock masses. International Journal of Rock Mechanics and Mining Sciences, 42, 2, 277-285. doi:10.1016/j.ijrmms.2004.09.015

Hoek, E., Read J., Karzulovic, A. and Chen, Z.Y. (2000): Rock slopes in civil and mining engineering. In: Proceedings of the International Conference on Geotechnical and Geological Engineering GeoEng 2000.

Hormazabal, E., Veramendi, R., Barrios, J., Zuniga Olate, G. and Gonzalez, F. (2013): Slope design at Cuajone Pit, Peru. In: PM Dight (ed.): Proceedings of the 2013 International Symposium on Slope Stability in Open Pit Mining and Civil Engineering- Australian Centre for Geomechanics, 527-539. doi:10.36487/acg_rep/1308_34_hormazabalo

ISRM (1981): Rock characterization, testing and monitoring – ISRM suggested methods. In: Brown E.T. (ed.): International Society of Rock Mechanics, Pergamon, Oxford.

Kayabasi, A. (2017): The Geological Strength Index Chart assesment for rock mass permeability. Bulletin of Earth Sciences Application and Research Centre of Hacettepe University, 38, 3, 295-309.

Lin, D., Sun, Y., Zhang, W., Yuan, R., He, W., Wang, B. and Shang, Y. (2014): Modifications to the GSI for granite in drilling. Bulletin of Engineering Geology and the Environment, 73, 4, 1245-1258. doi:10.1007/s10064-014-0581-0

Marinos, V. and Carter, T. (2018): Maintaining geological reality in application of GSI for design of engineering structures in Rock. Engineering Geology, 239, 282-297. doi:10.1016/j.enggeo.2018.03.022

Marinos, P. and Hoek, E. (2000): GSI: A geologically friendly tool for rock-mass strength estimation. In: Proceedings of GeoEng2000 Conference.

Marinos, V., Marinos, P. and Hoek, E. (2005): The Geological Strength Index: Applications and limitations. Bulletin of Engineering Geology and the Environment, 64, 1, 55-65. doi:10.1007/s10064-004-0270-5

Martin, D. and Stacey, P. (2013): Pit slopes in weathered and weak rocks. In: PM Dight (ed.): Proceedings of the 2013 International Symposium on Slope Stability in Open Pit Mining and Civil Engineering, Slope Stability 2013 - Australian Centre for Geomechanics, Perth, 3-28, 25 p. doi:10.36487/ACG_rep/1308_0.1_Martin

Mas Ivars, D., Deisman, N., Pierce, M. and Fairhurst, C. (2007): The synthetic rock mass approach - a step forward

in the characterization of jointed rock masses. In: Ribeiro e Sousa, Olalla, Grossmann (eds.): Proceedings of 11th Congress International Society of Rock Mechanics, 1, 485-490.

Mejía Camones, L. and Chacón Nuñez, C. (2019): Application of the Geological Strength Index in Peruvian underground mines: Retrospective 18 years after its implementation. In: Hadjigeorgiou, J. and Hudyma, M. (eds.): Proceedings of the Ninth International Symposium on Ground Support in Mining and Underground Construction – Australian Centre for Geomechanics, pp. 459–470, 12 p. doi:10.36487/acg_rep/1925_32_mejia

Mesec, J., Strelec, S. and Težak, D. Ground vibrations level characterization through the geological strength index (GSI). Rudarsko Geolosko Naftni Zbornik. 2016, 32, 1, 1-6. doi:10.17794/rgn.2017.1.1

Mostyn, G. and Douglas, K. (2000): The shear strength of intact rock and rock masses. In: Proceedings of GeoEng 2000: An International Conference on Geotechnical and Geological Engineering, Technomic Publishing, Lancaster, Pennsylvania, 23 p.

Pitts, M. and Diederichs, M. (2011): The effect of joint condition and block volume on GSI and rockmass strength estimation. In: Proceedings of 2011 Pan-Am CGS Geotechnical Conference, 6 p.

Read, J. and Stacey, P. (2009): Guidelines for open pit slope design. CSIRO Publishing - Melbourne, 512 p. doi: 10.1071/9780643101104

Riahi, A., Hammah, R.E. and Curran, J.H. (2010): Limits of applicability of the finite element explicit joint model in the analysis of jointed rock problems. In: Proceedings of the 44th ARMA conference, 10 p.

Russo, G. (2009): A new rational method for calculating the GSI. Tunnelling and Underground Space Technology, 24, 1, 103-111. doi:10.1016/j.tust.2008.03.002

Russo, A., Vela, I. and Hormazabal, E. (2020): Quantification of the intact Geological Strength Index for rock masses in hypogene environment. In: Castro, R, Báez, F. and Suzuki, K. (eds.): Proceedings of the Eighth International Conference and Exhibition on Mass Mining (MassMin 2020) – University of Chile, 1188-1201, 14 p. doi:10.36487/acg_repo/2063_87

Shang, Y., Zhang, W. and Lu, Y. (2011): Drilling Geological Strength Index in altered gneiss. Harmonising Rock Engineering and the Environment, 707-710, 4p. doi:10.1201/b11646-127

Schlotfeldt, P., Elmo, D. and Panton, B. (2018): Overhanging rock slope by design: An integrated approach using rock mass strength characterisation, large-scale numerical modelling and limit equilibrium methods. Journal of Rock Mechanics and Geotechnical Engineering, 10, 1, 72-90.

Schlotfeldt, P. and Carter, T.G. (2018): A new and unified approach to improved scalability and volumetric fracture intensity quantification for GSI and rockmass strength and deformability estimation. International Journal of Rock Mechanics and Mining Sciences, 110, 48-67. doi:10.1016/j.ijrmms.2018.06.021

Sonmez, H. and Ulusay, R. (1999): Modifications to the Geological Strength Index (GSI) and their applicability to stability of slopes. International Journal of Rock Mechanics and Mining Sciences, 36, 6, 743-760. doi:10.1016/s0148-9062(99)00043-1

Sonmez, H. and Ulusay, R. (2002): A discussion on the Hoek - Brown failure criterion and suggested modifications to the criterion verified by slope stability case studies. Bulletin of Earth Sciences Application and Research Centre of Hacettepe University, 26, 1, 77–99.

Sonmez, H., Ulusay, R. and Gokceoglu, C. (1998): A practical procedure for the back analysis of slope failures in closely jointed rock masses. International Journal of Rock Mechanics and Mining Sciences, 35, 2, 219-233. doi:10.1016/s0148-9062(97)00335-5

Sonmez, H., Ercanoglu, M., Ozcelik, Y. and Dagdelenler, G. (2021): How reliable are hand calculation methods used for selection of strength of geomaterials for slope design?. In: Workshop "Rockmass Characterization with Emphasis in Rock Slope Hazard". Commission 38 (C38-IAEG) in 3rd European Regional Conference of IAEG.

Špago, A. and Jovanovsky, M. (2019): Applicability of the Geological Strength Index (GSI) classification for carbonate rock mass. In: Proceedings of Geotechnical challenges in karst –ISRM Specialised Conference, 7 p.

Truzman, M. (2009): Metamorphic rock mass characterization using the Geological Strength Index (GSI). In Proceedings of the 43rd U.S. Rock Mechanics Symposium & 4th U.S. - Canada Rock Mechanics Symposium – American Rock Mechanics Association (ARMA), 6 p.

Tsiambaos, G. and Saroglou, H. (2009): Excavatability assessment of rock masses using the geological strength index (GSI). Bulletin of Engineering Geology and the Environment, 69, 1, 13-27. doi:10.1007/s10064-009-0235-9

Xia, L., Zheng, Y. and Yu, Q. (2016): Estimation of the REV size for blockiness of fractured rock masses. Computers and Geotechnics, 76, 1, 83-92.

SAŽETAK

Optimizirani geološki indeks čvrstoće (GSI) primijenjen u analizi stabilnosti kosina u stijenskim masama

Velik broj analiza stabilnosti kosina promatra diskontinuirane stijenske mase u kojima je GSI (geološki indeks čvrstoće) procijenjen na razini izdanka smatran ulaznim podatkom za definiranje čvrstoće stijenske mase. Međutim, taj je postupak neprikladan kada su veličina izdanka i veličina kosine znatno različiti (npr. kosine površinskoga kopa), što rezultira precijenjenom čvrstoćom stijenske mase. Iz toga razloga, a u nedostatku kriterija za izmjenu GSI-ja na temelju učinaka razmjera, u ovome istraživanju predlaže se nova verzija GSI-ja, nazvana GSI_e ili optimizirani GSI. Da bi se definirao izraz za dobivanje optimiziranoga GSI-ja u smislu svojstava stijenske mase, provedene su analize komparativne stabilnosti u nizu hipotetskih kosina pomoću dvaju pristupa: prvi smatra stijensku masu diskontinuiranom, a drugi smatra stijensku masu ekvivalentnim kontinuiranim medijem koji karakterizira optimizirani GSI. U obama pristupima slični su faktor sigurnosti i površina sloma za odgovarajuću optimiziranu vrijednost GSI-ja procijenjenu u svakoj analiziranoj kosini. U skladu s rezultatima predložen je oblik GSI_e koji se koristi visinom kosine, razmakom, čvrstoćom intaktnoga stijenskog materijala, postojanošću i svojstvima diskontinuiteta. Na kraju je provedena validacija toga oblika primjenom u pet slučajeva rudarskih kosina na kojima je došlo do sloma.

Ključne riječi:
učinak mjerila, GSI, stijenska masa, mehanika stijena, stabilnost kosina, geomehanička karakterizacija

Author's contribution

The author prepared the whole work.